IGM88AP-205-726-G
CNRC 28906

AGEING CHA[illegible]RISTICS OF DENDRITIC AND NON-DENDRITIC (STIR-CAST) Zn-Al ALLOY (ZA-27)

by

H. LeHuy
Industrial Materials Research Institute
75 De Mortagne Blvd.
Boucherville (Quebec) Canada
J4B 6Y4

and

G. L'Espérance
Department of Metallurgical Engineering
École Polytechnique de Montréal
P.O. Box 6079, Succ. "A"
Montreal (Quebec) H3C 3A7

ABSTRACT

The dimensional changes of dendritic and non-dendritic (stir-cast) Zn-Al alloy (ZA-27) were investigated during ageing at temperatures in the range 20-245°C. The linear expansion of both dendritic and non-dendritic samples increased rapidly with ageing time after about 1 day at 95°C. An initial normalisation treatment led to a large initial growth of the alloy which increased further after prolonged aging times ($\gtrsim 10^3$ hours). Accelerated ageing tests in the range 75-250°C showed that increasing the ageing temperature decreased the long term linear expansion of the alloy. In comparing the behaviour of the two materials, the stir-cast material grew less than the dendritic alloy. Extensive SEM and TEM done on as-stir-cast and aged samples showed that the main changes during ageing occurred in the α (FCC) lamellae of the β eutectoid, the α phase at the primary α particles/β eutectoid interface and in the interparticle areas. In the α lamellae and at the interface, zinc precipitated whilst the τ' phase precipitated in the interparticle areas. It is considered that the occurrence of this latter phase, rich in copper, is responsible for the growth of stir-cast material during ageing.

1. Introduction

Among the zinc-aluminium foundry alloys, ZA-27 exhibits attractive physical and mechanical properties combined with good friction and wear resistance properties making it a choice alloy for a multitude of end-use applications. As some of these applications require increased performance of the alloy at high temperature, in particular its dimensional stability, intensive investigations [1] have been done to develop high quality products. Recently, non-conventional casting processes, such as stir-casting (or rheocasting) [2-4] and compocasting [5] were investigated for ZA-27 taking advantage of this alloy's wide freezing range. As the solidification conditions in these techniques are not standard, a different behaviour of the microstructure of the alloy was reported.

The microstructural changes of the binary Zn-Al alloy during ageing already have been followed by Lecomte-Beckers et al. [6]. Their work pointed out a multi-stage decomposition of supersaturated solid solutions. The presence of 2.3 wt% copper in ZA-27 induces a complex microstructure with several metastable phases which are strongly related to the solidification conditions. X-ray analysis [7] on aged as-cast alloy revealed a multiphase decomposition with the precipitation of τ' phase rich in Cu and Al.

The complexity of the microstructure of stir-cast alloy, composed of degenerated dendrites embedded in a residual liquid, leads us to search further for a better understanding. Dimensional changes of both dendritic and non-dendritic (spheroidized) alloys were followed at different holding

temperatures varying from room temperature to 245°C. Their microstructural changes were studied by scanning and transmission electron microscopy. Results showed that the linear expansion of ZA-27 on ageing could be minimized in stir casting by promoting the formation of stable α phase. This paper describes the ageing behaviour of this material.

2. Experimental procedures

2.1 Material preparation

The starting material for this study was a commercial ZA-27 alloy used for casting applications. Its nominal composition, solidification characteristics and phases are given in Table 1. Two types of structure were selected for this investigation: a material conventionally cast in a graphite mould and a material stir cast at 470°C. Conventional casting was carried out by melting 10-kg batches of the alloy in an electric furnace. The melt was then cast in a graphite mold with 50 degrees of superheat. The castings were well insulated in order to produce an equiaxed dendritic structure (Fig. 1a). On the other hand, stir casting was effected in an inert-gas-protected rheocaster with casting also in a graphite mould. Details of the stir casting technique have already been published [3]. At 470°C, stir-cast material exhibits 30% volume primary particles as shown in Fig. 1b.

Immediately after casting, some ingots were stabilized by a normalization heat treatment of 12 hours at 250°C.

2.2 Measurements of dimensional changes

The dimensional variation of aged alloys was determined by measuring the change in length of cylindrical specimens. Accelerated ageing from 175 to 245°C was carried out with a computerized Theta Dilatronic dilatometer on specimens 0.3 cm in diameter and 5.0 cm in length. The dimensional change was measured by an LVDT with 1% accuracy and the temperature of the holding furnace was monitored within ±1°C.

Ageing tests at 95°C were conducted by placing specimens 3.8 cm in diameter and 10 cm in length in a muffle furnace. In this case, the linear expansion was measured at room temperature using a micrometer after specimens had been cooled in air. They were then replaced in the furnace for a further period of ageing. Finally, the test results were compared to reference measurements of material held at room temperature.

2.3 Scanning and transmission electron microscopy

Scanning and transmission electron microscopy (SEM and TEM) were used to characterize the phases present in each of the samples and to follow the microstructural changes which occurred during ageing. Samples for the SEM were prepared by conventional mechanical polishing techniques and observed in the unetched condition. Samples for TEM were prepared by ion beam thinning. Initially, 3 mm discs were ground flat on SiC paper down to a thickness of 150 μm. Micro profiles were then obtained for both faces using a micro dimpler so that the remaining thickness in the center of the disc was considerably

reduced. Final polishing in the ion beam thinner was done with a specimen holder cooled with liquid nitrogen and using both ion guns at 50° operated at 6 KV and a current of 0.2 μ Amp. When perforation of the discs occurred, the angle was reduced to 10° so as to increase the area transparent to electrons. The overall final polishing in the ion thinner required approximately 15 hours.

Backscattered electron images (BEI) in the SEM were particularly useful for identifying and rapidly locating the different phases present in the structure of the samples in view of the considerable chemical contrast difference between the various phases. Electron diffraction and X-ray microanalysis were the main methods used to identify the phases in TEM.

Due to the considerable effort needed and time involved between the observations of the samples in the TEM and the subsequent indexing of the patterns and positive identification of the phases, BEI pictures in the SEM were often initially taken of the polished TEM discs prior to observations in the TEM. These pictures reduced considerably the time needed to identify the different phases and allowed rapid location of the phases of interest during the observations in the TEM. In addition, a sequence of BEI images of the perforated thin foils at regular intervals during ion beam thinning allowed systematic thinning of the samples until a desired phase was located near the edge of the hole of the disc. This was particularly useful for locating and characterising the interface between the α and β phases.

X-ray microanalysis in the TEM was carried out at 200 KV with a probe of

similar (or smaller) size than that of the phase analysed. The net intensity was obtained using the spectrum itself to fit the background and the concentration in each element calculated using a standardless quantification program written in our laboratory based on a widely accepted procedure [8-9]. The errors associated with such quantification procedure are in the range 5-10% [10]. Errors below 5% may have been achieved by the use of single phase standards of known composition. Such standards were not readily available for this study.

3.0 Results

3.1 Dimensional changes

3.1.1 Dimensional changes versus ageing temperature

Fig. 2 shows the dimensional changes of dendritic and non-dendritic specimens aged at room temperature and 95°C. Four experimental curves are presented in each graph, corresponding to different test conditions: respectively the room temperature tests on as-cast (curve A) and normalized (curve NA) materials and the 95°C ageing tests on as-cast (curve F) and normalized (curve NF) materials. For these tests, the linear expansion was followed during 10^4 hours (~ 1½ years). Data show that, for both dendritic and non-dendritic as-cast alloys, ageing at 20°C causes a slight shrinkage of 0.02% after 400 days (curves A); at this temperature, the stir-cast material seems more stable than the conventional ones. This feature will be discussed in detail in the next section. With regards to the tests performed at 95°C, the curves show a rapid initial shrinkage after 1 ageing day followed by a

pronounced expansion (curves F). On the other hand, the normalization treatment of 12 hours at 250°C, applied to both materials, induced an initial growth of about 0.09%. However the transformation was not complete, as shown by the NF curves in Fig. 2, in which it is seen that the linear dilatation continued to increase slightly.

Accelerated ageing tests were performed at several temperatures ranging from 175°C to 245°C for times up to 100 hours. The results, shown in Fig. 3a for dendritic material and in Fig. 3b for non-dendritic material, indicate that increasing the ageing temperature decreases the long-term linear expansion of the alloy. However, above 228°C, the linear expansion passes through a maximum, then decreases slightly. No satisfactory explanation has been given yet, but probably at high temperature two phenomena occur in opposition: the phase transformation causes the metal to expand, whereas the structural defects formed during solidification are eliminated by sintering effects, producing shrinkage. Unfortunately, during testing at high temperature, the dimensional changes indicate the resultant of these two phenomena.

As the observed linear variations during ageing treatments are the resultant of thermally activated phenomena, it is assumed that an Arrhenius-type law is applicable to describe the process, i.e.:

$$t = t_o \exp \left\{ - \frac{Q}{RT} \right\} \qquad (1)$$

where t (hours) is the ageing time corresponding to the maximum of linear

variations;

Q (Kcal/mole), the apparent activation energy of the process;

R the Boltzmann constant;

T (K) the heat treating temperature;

and t_o a constant.

Figure 4 shows a plot of the ageing time versus 1/T. Additional results from the literature [1,11] are also presented in the same figure. The activation energy Q described by equation (1) is then given by the slope of the fitting curve. For ZA-27 alloy, the calculated value of the activation energy is equal to 19 Kcal/mole in the range of 75-250°C. From consideration of activation energy data for metal diffusion, it appears that the dimensional changes of ZA-27 in ageing are controlled by the diffusion of elements. Indeed, the activation energy of diffusion of Zn in Zn-rich homogeneous aluminium alloys is reported [12] equal to 20 Kcal/mole and in the Cu-Zn system, the values of Q in γ phase [13] are in the range of 17-25 Kcal/mole.

3.1.2 Dendritic versus non-dendritic structure transformations

The experimental data show a slight difference between the dendritic and non-dendritic structures. Linear expansion of the dendritic specimen aged at 95°C was about 0.14% after 10^4 hours ageing (curve F, Fig. 2a) while the stir-cast material expanded by 0.10% under the same conditions, as shown by curve F, Fig. 2b. The same difference can be seen for the accelerated ageing tests described in the previous section (curves NF in Fig. 3a and 3b). Examining the behaviour of the two types of structure, Mykura et al. [14] have

pointed out an opposite behaviour, whereby it was reported that the stir-cast material grew slightly more than the dendritic one. The reasons for the distinctly contrary results are not clear, but it is possible that the different techniques of slurry production could explain this disagreement. Effectively, the two techniques adopted by Mykura and in the present work to stir the solid-liquid alloy were not the same. Moreover the important casting stage after stirring used in both cases also differed. In Mykura's work, the slurry was cast in a hot steel mould, while our material was poured in a graphite one. The cooling rate in the two cases was different. In order to clarify the process of phase transformation which induced the linear expansion, comparative microstructural studies were carried out.

3.2 Microstructural studies

3.2.1 Structure of as-cast materials

Figure 5 shows backscattered electron images (BEI) of as-cast dendritic and non-dendritic materials, revealing the multiphase character of ZA-27. In both micrographs, the dark zone (marker G) is the α phase formed in the centre of the dendrite or the core of the primary particles. The grey zone (markers D and F) in the pictures, corresponding to the β constituent, reveals a fine lamellar structure of a eutectoid decomposition. The interdendritic or interparticle areas (markers A and B) appearing bright in the BEI micrographs must contain large amounts of the relatively heavy elements in the alloy (Cu and Zn). The phases expected from the ternary Zn-Cu-Al phase diagram [15] are mainly the Zn rich ε and η phases.

3.2.2 Ageing effects on microstructural changes

Fig. 6 shows microstructures of normalized materials after a heat treatment at 250°C for 12 hours. This condition corresponds to the NA treatment in Figure 2 and is thus for samples which underwent ≈ 0.08% dilatation. The initial phases of as-cast alloys, α, β, η and ε, which are formed as supersaturated phases, tended to transform into more stable phases during ageing. These transformations changed the microstructural aspect of the alloy. Coarse precipitates were observed at the interface of α/β phases (marker H), while the eutectoid structure of former β phase tended to spheroidize (markers D and F) and fine particles precipitated in the interparticle area (markers A and B). All these transformations were found to be the same to a varying degree in aged specimens. In order to describe thoroughly these phase transformations, fine microstructural and diffraction pattern analysis were undertaken with transmission electron microscopy.

3.3 Fine microstructural and diffraction pattern analysis

Figure 7a shows a TEM micrograph of a sample as stir cast. The α phase (marker A) as well as the β phase (marker B) and the interface α/β can be clearly identified in the figure. Although there were some areas of the α phase for which no precipitation was observed, very extensive precipitation was generally observed in the α phase. As seen clearly at a higher magnification (Fig. 7b), most of the precipitates are thin (≈ 0.02 μm) and elongated (1.5 - 2.0 μm) while others are small and spherical (≈ 0.35 μm in diameter).

Figure 7c shows a composite diffraction pattern from the primary α phase and the precipitates. In this pattern, spots 1 to 5 can be indexed as the {220} reflections of the [111] pattern of the primary aluminium-rich alpha phase. In addition, spots 7 to 12 can all be indexed as reflections from pure zinc contituting the [0001] pattern of that phase. All the other satellite spots arise from double diffraction effects as shown by the fact that they disappear when tilting the specimen about an axis joining these spots to the central transmitted beam.

The coarser precipitates (≈ 1.5 μm long and 0.2 μm wide) seen at the α_p/β interface are also zinc with some copper in solution; X-ray microanalysis showed them to be 96 Zn-2Cu-2Al. In assessing these compositions, account should be taken of the fact that the analyses were performed with the precipitates embedded in the Al matrix which will affect the results because of beam overlap onto the matrix. Nevertheless, copper was consistently detected in the precipitates while analyses of the matrix showed that it contained very little copper.

On the other hand, the lamellar structure of the β constituent is shown in Figure 8. The crystal structure of the lamellae determined by parallel illumination electron diffraction was found to be FCC for the lamellae marked F and HCP for the lamellae marked H in the micrograph. X-ray microanalysis with the results given in Table 2 showed that the β phase is in fact constituted of lamellae of the α (FCC, Al-rich) and η (HCP, Zn-rich) phases as expected from the binary Zn-Al phase diagram. No precipitation was observed in these lamellae contrary to the extensive precipitation seen in the primary

α particles. Some α lamellae, however, had begun to tranform as shown by the presence of small grains in some of the lamellae.

Finally, the interparticle area is shown to be constituted of a large number of small equiaxed grains (0.1 μm, Fig. 9). Microanalysis of individual grains with a small probe showed that most of the grains contained a very small amount of aluminium (≈ 2.0 at %) and that the Cu/Zn ratio varied from 0.13 to 0.24. The latter value corresponds almost exactly to that of the $CuZn_4$ phase and it was also obtained in the case of an analysis carried out with a 0.5 μm probe covering ≈ 5 grains. It is therefore considered that the phase constituting the interparticle area is mainly $CuZn_4$.

3.4 Effect of a high temperature ageing treatment

Figure 10a shows a typical area of the primary α particles after ageing. Both elongated and spherical precipitates of similar dimensions to those in the as-cast sample (Fig. 7b) were observed. Some areas of the primary α particles, however, contained only spherical precipitates (Fig. 10b) indicating that in some areas the elongated precipitates had undergone complete spheroidization. When this was the case, much smaller precipitates (≈ 50 nm) could be seen in the background. It is likely that spheroidization of the long and thin precipitates was more nearly complete in the aged samples than in the as-cast samples although more observations of different areas would be needed to confirm this.

Composite diffraction patterns of the α matrix and of the precipitates

were identical to those obtained for the as-cast sample (Fig. 7c) indicating that the precipitates were zinc. Thus, the microstructure of the α particles after ageing was very similar to that of the samples prior to ageing.

Figure 11 is a portion of the interface between the α_p particles and the β eutectoid. As in the case of the as-stir-cast sample, some coarse zinc precipitates (≈ 1 μm) can be seen along the interface. A comparison of that figure with Fig. 7a from the as-cast sample shows that the main change at the interface during ageing was the occurrence of copious precipitation in the α regions of the interface.

Such precipitation also occurred in the α lamellae of the β eutectoid (marker B in Fig. 11). A higher magnification micrograph of one α lamella is shown in Fig. 12 along with a [111] diffraction pattern from the aluminium matrix. Clearly, the pattern is identical to those obtained for the primary α particles (Fig. 7) which shows that the precipitates formed in the α lamellae during ageing are zinc.

Ageing also led to a significant transformation of the interparticle areas. These areas, of a composition determined to be close to that of $CuZn_4$, in the as-cast condition transformed upon ageing into a matrix of zinc containing very little amounts of copper and aluminium in solution (Table 3) and a large number of precipitates approximately 0.2 μm in size (Fig. 13). In some cases, precipitates were actually sticking out from the edge of the hole of the foil thereby allowing X-ray analysis and electron diffraction of the precipitates without any contribution from the matrix. Both the chemical

composition (Table 3) and the indexation of the diffraction pattern show the precipitates to be the τ' phase studied by Murphy [7] with a composition of 31.3 Al-56.1 Cu-12% Zn and a rhombohedral structure with $a = b = c = 0.8676$ nm and $\alpha = \beta = \gamma = 27.41°$.

4. Discussions

The solidification conditions during stir casting are quite different from those during conventional casting. In stir casting, the percentage of primary particles,formed during the stirring stage, i.e. the α phase which is in the present study approximately 30% of the total volume of the alloy, is much larger than that obtained in dendritic cast material. In addition, the cooling rate of the stirring stage is generally low [17], i.e. between 1°C/min and 10°C/min with usually a holding time of a few minutes prior to casting. The influence of these casting parameters on the structure of stir-cast materials has been discussed in earlier work [3]. Thus under these conditions, the α phase supersaturation of the primary particles would not be as high as inside the dendrites of conventional casting. The subsequent heat treatment should not change its structure. On the other hand, the second stage of solidification of the slurry occurred when the liquid-solid metal was poured into the mould, i.e. at a temperature well below the liquidus. Therefore, the supersaturation of zinc content in α lamellae must have been high. Subsequent heat treatment induced profound changes in the α lamellae by precipitation of the excess zinc. Mykura et al. [11] pointed out this decomposition reaction $\alpha_{supersaturated} \rightarrow \alpha + \eta$ as a short term transformation. As the presence of copper in solution increases the time of

transformation [18], our results showed that it could hardly be achieved at room temperature so that heat treatments at a moderately raised temperature are needed to induce the reaction. As this transformation is associated with the slight contraction in the early stages of ageing, stir-cast materials with the presence of stable α primary particles are less influenced.

On the other hand, the long term phase transformations, which produce dimensional growth, are associated [16] with two distinct reactions. One is the four-phase reaction transforming the copper-rich metastable epsilon phase into the equilibrium τ' phase as discussed in section 3.4. The other is due to the reduction of copper content in solution in the Zn-rich phase. In stir-cast alloy, copper is concentrated in the interparticle areas whereas the α primary particles and β constituent are leaner in copper than in the equivalent dendritic material and are by this fact less influenced by the η HCP growth. Therefore, the transformation of the interparticle areas with formation of τ' as shown above seems to be the main reason for the growth in aged stir-cast materials.

5. Conclusions

Phase transformation of as-cast (dendritic and non-dendritic) ZA-27 alloy during isothermal treatment is the resultant process of decomposition of several supersaturated phases. In the first stage, the FCC aluminium-rich phase decomposes into the equilibrium η and α phases. Our results clearly show this decomposition reaction to be a short term transformation, inducing a slight contraction when the cast material is cooled down and/or in the early

stages of ageing.

The long term phase transformations, which produce dimensional growth, are associated with the formation of equilibrium τ' phase in the interdendritic (or interparticle) phases and to the reduction of copper content in solution in the Zn-rich phase.

In stir-cast material, the dimensional growth is slightly lower than that of conventionally cast material. It is tempting to associate this behaviour with the presence of more stable phases in primary particles and in the β constituent.

ACKNOWLEDGEMENTS

The authors would like to express their appreciation to Gilles St-Amand for his technical assistance and their acknowledgements to Dr. D.C. Briggs of CANMET for his invaluable advice.

REFERENCES

1- Engineering Properties of Zinc Alloys, publ. by Int. Lead Zinc Res. Org. Inc., 2nd Ed., (1981), New-York.

2- S.Murphy, T. Savaskan and J.K. Wheeldon, in Proc. Conf. "Casting and Foundry Technology", Univ. of Aston, Birmingham, U.K., Sept. 1981, Int. Congress on Metals Engineering, Paper 7.

3- H. LeHuy, J. Masounave and J. Blain, J. of Mat. Sc., 20, (1985), 105-113.

4- J. Collot, In. Proc. Int. Symposium on Zinc-Aluminium (ZA) Casting Alloys, 25th Annual Conference of Metallurgists, Toronto, August 1986, CIM Series 25-5/1, N° 1, 249-261.

5- R. Guerriero, J.B. Parse and I. Tangerini, as ref. 4, 229-246.

6- J. Lecomte-Beckers, L. Terziev, J. Wegria and T. Greday, as ref. 4, 35-43.

7- S. Murphy, Metal Science, 9, (1975), 163-168.

8- D.B. Williams, "Practical Analytical Electron Microscopy in Materials Science", Philips Electron Instrument, Inc., Electron Optics Publishing Group, New Jersey, 1984.

9- M.H. Loretto, "Electron Beam Analysis of Materials", Chapman and Hall, London, 1984.

10- J.E. Wood, D.B. Williams and J.I. Goldstein, Journal of Microscopy, 133, (1984), 255-274.

11- N. Mykura, Y.H. Zhu and S. Murphy, Canadian Met. Quarterly, 25, (1986), 151-159.

12- J.E. Hilliard, B.L. Averbach and Morris-Cohen, Acta Met., 7, (1959), 86-92.

13- R.F. Mehl and C.F. Lutz, Trans. of the Met. Soc. of AIME, 221, (1961), 561-567.

14- N. Mykura and S. Murphy, as ref. 4, 45-55.

15- Phase diagrams, Metals Handbook, ASM, 8th Edition, Vol. 8, (1973), 390-391.

16- N. Mykura, S. Murphy and Y.H. Zhu, Mat. Res. Soc. Symp. Proc., 21, (1984), 841-844.

17- H. LeHuy, J. Blain and J. Masounave, as ref. 4, 143-153.

18- A.E. Smith and G.A. Hare, J. Inst. Metals, 101, (1973), 320.

FIGURE CAPTIONS

Table 1: Characteristics of the Zn-Al alloys studied.

Table 2: Results of the X-ray microanalysis of the lamellae of the β eutectoid before ageing.

Table 3: Results of the X-ray microanalysis of the constituents of the interparticle areas after ageing.

Figure 1: Microstructure of as-cast materials:
a) dendritic
b) stir-cast

Figure 2: Dimensional changes of ZA-27 with ageing time under various test conditions.
a) dendritic
b) non-dendritic
- curve A: as-cast specimen, at room temperature
- curve F: as-cast specimen, at 95°C
- curve NA: normalized specimen, at room temperature
- curve NF: normalized specimen, at 95°C
(N.B.: 0/00 means per thousand).

Figure 3: Dimensional changes of ZA-27 during accelerated ageing tests, respectively at 175°, 206°, 228° and 245°C during 100 hours.
a) dendritic
b) stir-cast

Figure 4: Arrhenius plot of ageing time versus 1/T.

Figure 5: Backscattered electron images of as-cast materials showing the different phases present.
a) dendritic
b) stir-cast.

Figure 6: Backscattered electron images of normalized specimens (250°C - 12 hours) showing the transformation products:
a) dendritic
b) stir-cast.

Figure 7: a) Transmission electron micrograph (TEM) showing a general view of the structure of primary alpha particle (A), the interface α_p/β (C) and the β constituent (B) of an as-stir-cast sample.

b) Higher magnification micrograph to show the morphology of the precipitates.

c) Composite electron diffraction pattern from the primary α particle and the precipitates.

d) Indexation of the diffraction pattern shown in c.

Figure 8: TEM micrograph of the lamellar structure of the β constituent of an as-stir-cast sample.

Figure 9: Appearance of the interparticle area in the as-stir-cast sample.

Figure 10: a) Microstructure of the primary α particles after a high temperature ageing treatment.

b) Area of a primary α particle containing only spherical precipitates. Note the presence of very small precipitates (≈ 50 nm) in the background.

Figure 11: Micrograph of the interface between the primary α particles and the β eutectoid after ageing. Copious precipitation occurred during ageing in the α regions of the interface (marker C) and in the α lamellae of the β eutectoid (marker B).

Figure 12: TEM micrograph of an α lamellae of the β constituent showing the extensive precipitation that occurred during ageing.

Figure 13: Micrograph of the interparticle areas after ageing showing precipitates approximately 0.2 μm in size formed in a matrix of almost pure zinc.

Table 1: Characteristics of the Zn-Al alloys studied

- **Base alloys**
  - Composition of ZA-27: 25-28 Al; 2-2.5 Cu; 0.15 Mg
    bal. Zinc (wt%)
  - Temperature:
    - Liquidus: 492°C
    - Eutectic: 382°C
    - Eutectoid: 275°C

Casting conditions	Type	Dimensions (μm)
Superheat castings	100% coarse dendrites	100 - 200
Stir-cast 475°C	70% fine dendrites	<25
	30% primaries	100 - 500

Table 2: Results of the X-ray microanalysis of the lamellae of the β eutectoid, before ageing.

PHASE	% Al (at. %)	% Zn (at. %)	% Cu (at. %)
α LAMELLAE	72	24	4
η LAMELLAE	5	90	5

Table 3: Results of the X-ray microanalysis of the lamellae of the interparticle areas after ageing.

MICROSTRUCTURAL CONSTITUENT	% Al (at. %)	% Cu (at. %)	% Zn (at. %)
MATRIX	1%	1%	99
PRECIPITATE	22	64	14

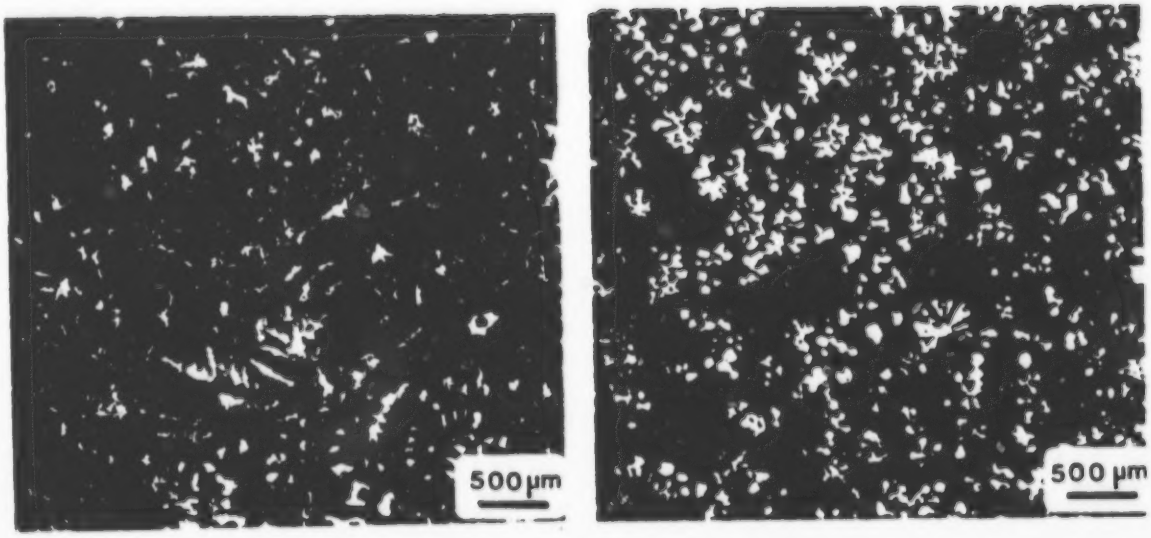

a) b)

Figure 1: Microstructure of as-cast materials:
a) dendritic
b) stir-cast

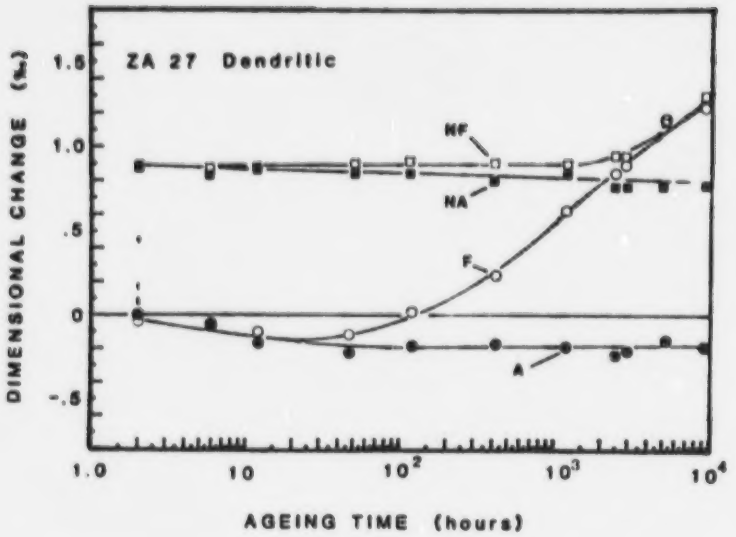

a)

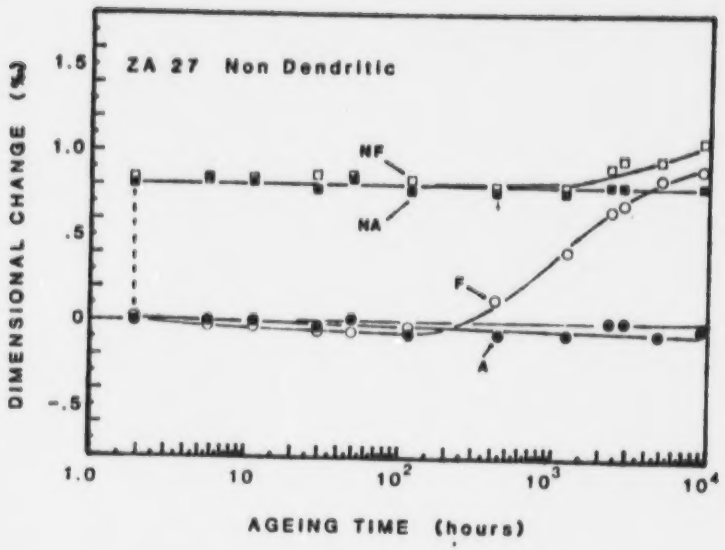

b)

Figure 2: Dimensional changes of ZA-27 with ageing time under various test conditions.
a) dendritic
b) non-dendritic
- curve A: as-cast specimen, at room temperature
- curve F: as-cast specimen, at 95°C
- curve NA: normalized specimen, at room temperature
- curve NF: normalized specimen, at 95°C
(N.B.: 0/00 means per thousand).

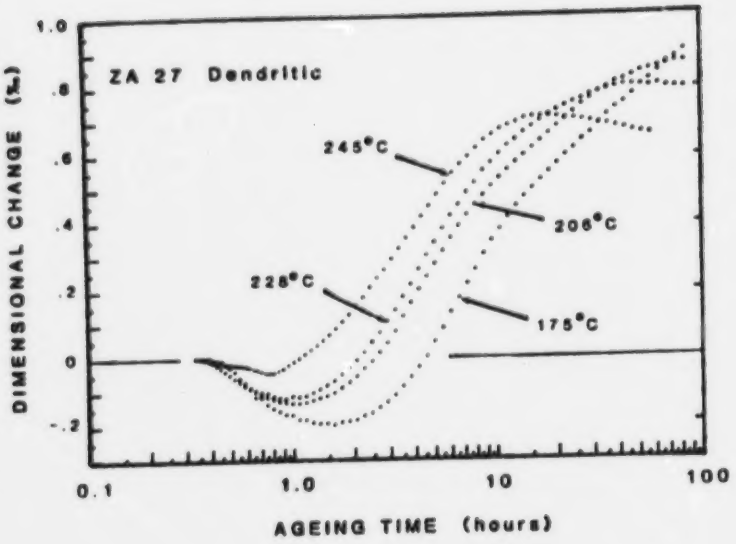

a)

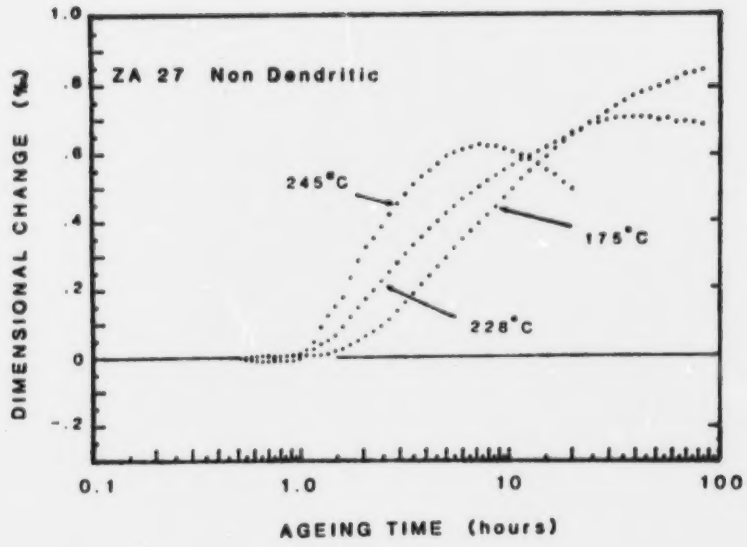

b)

Figure 3: Dimensional changes of ZA-27 during accelerated ageing tests, respectively at 175°, 206°, 228° and 245°C during 100 hours.
a) dendritic
b) stir-cast

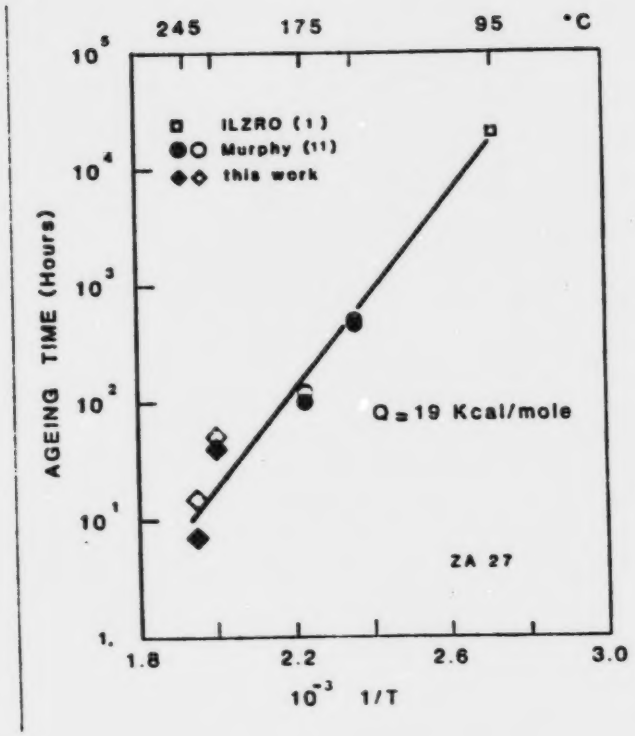

Figure 4: Arrhenius plot of ageing time versus 1/T.

a) b)

Figure 5: Backscattered electron images of as-cast materials showing the different phases present.
a) dendritic
b) stir-cast.

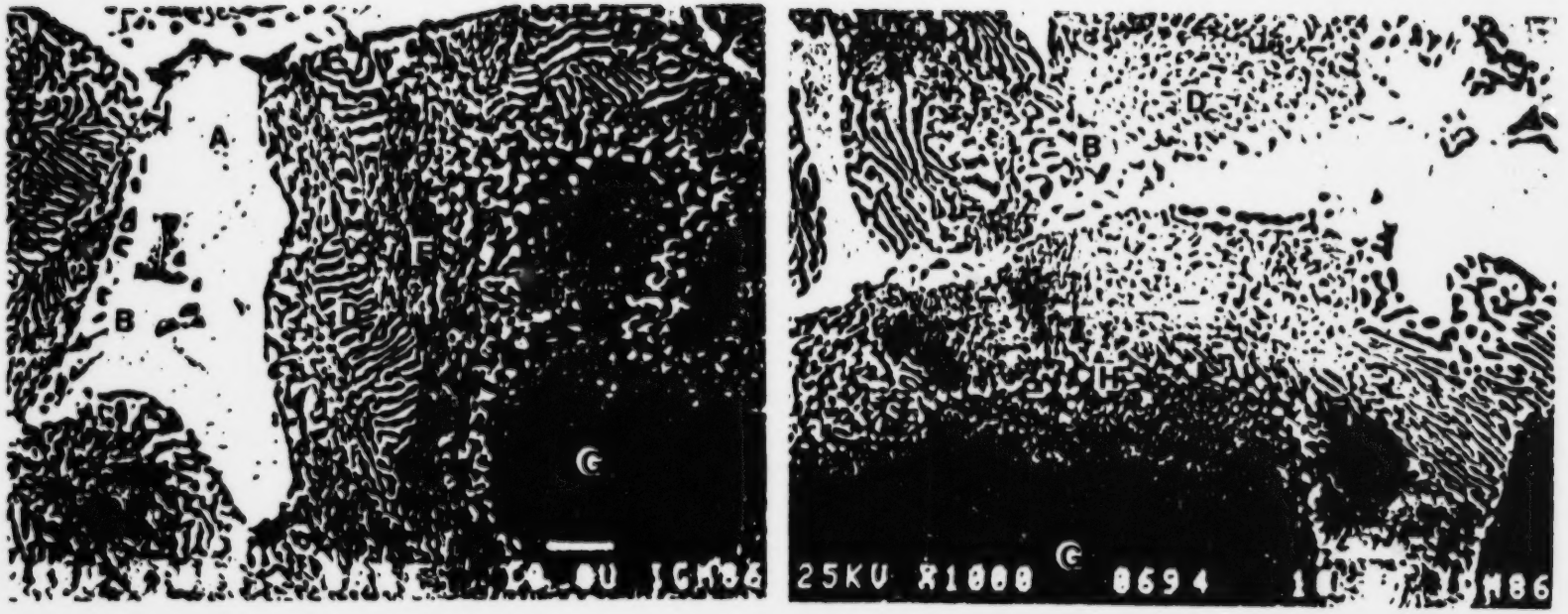

a)

b)

Figure 6: Backscattered electron images of normalized specimens(250°C - 12 hours) showing the transformation products:
a) dendritic
b) stir-cast.

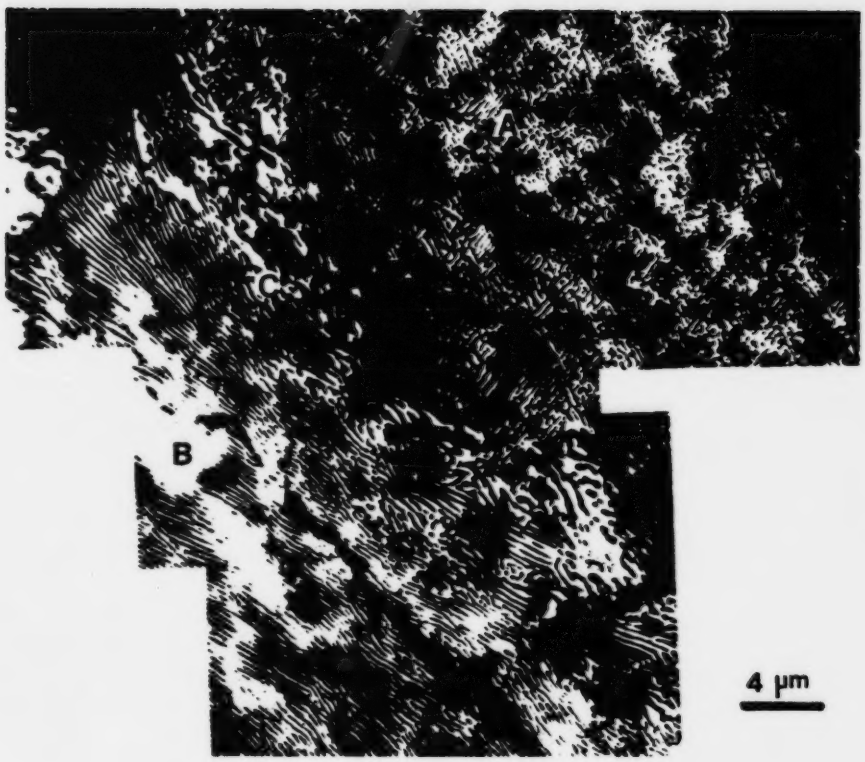

a)

Figure 7: a) Transmission electron micrograph (TEM) showing a general view of the structure of primary alpha particle (A), the interface α_p/β (C) and the β constituent (B) of an as-stir-cast sample.

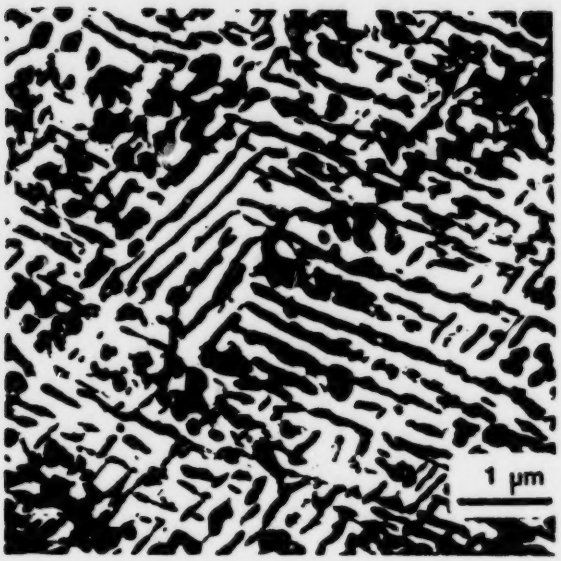

b)

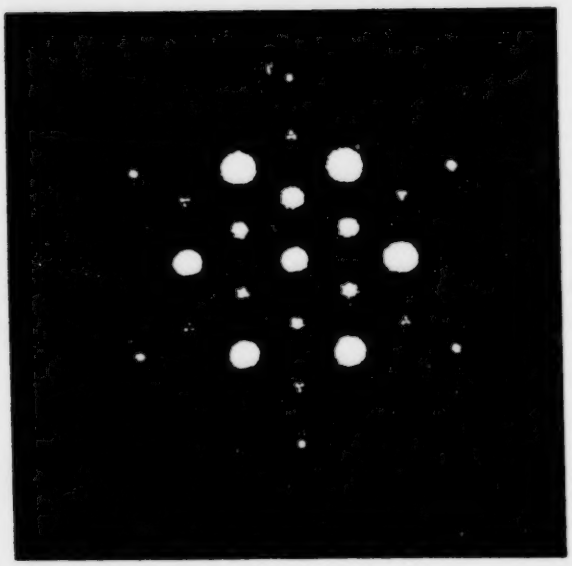

c)

d)

Figure 7: b) Higher magnification micrograph to show the morphology of the precipitates.

c) Composite electron diffraction pattern from the primary α particle and the precipitates.

d) Indexation of the diffraction pattern shown in c.

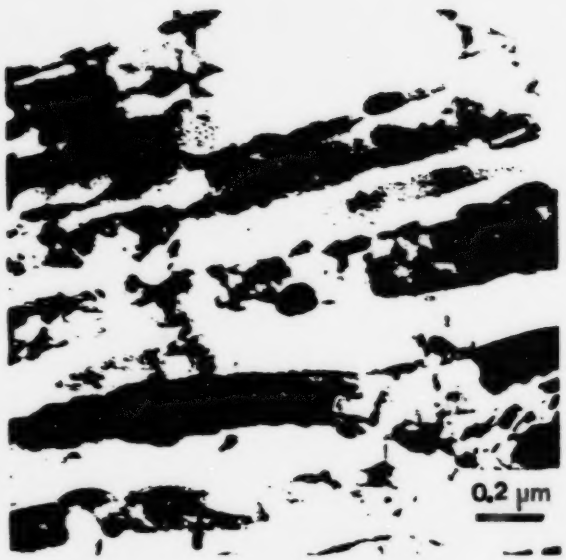

Figure 8: TEM micrograph of the lamellar structure of the β constituent of an as-stir-cast sample.

Figure 9: Appearance of the interparticle area in the as-stir-cast sample.

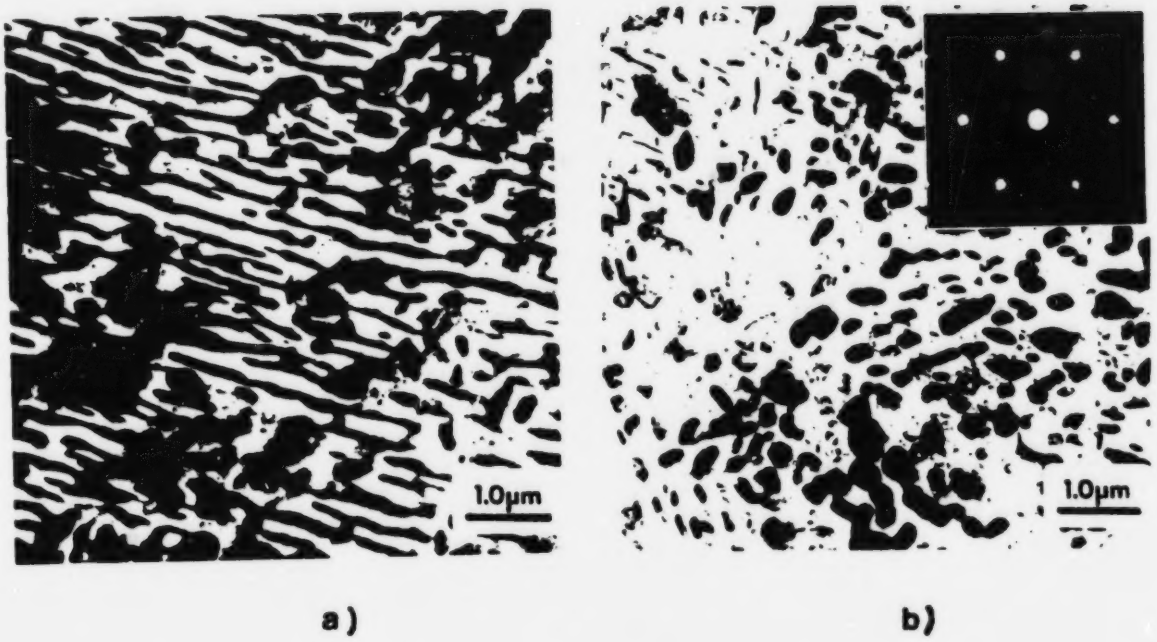

Figure 10: a) Microstructure of the primary α particles after a high temperature ageing treatment.

b) Area of a primary α particle containing only spherical precipitates. Note the presence of very small precipitates (≈20nm) in the background.

Figure 11: Micrograph of the interface between the primary α particles and the β eutectoid after ageing. Copious precipitation occurred during ageing in the α regions of the interface (marker C) and in the α lamellae of the β eutectoid (marker B).

Figure 12: TEM micrograph of an α lamellae of the β constituent showing the extensive precipitation that occurred during ageing.

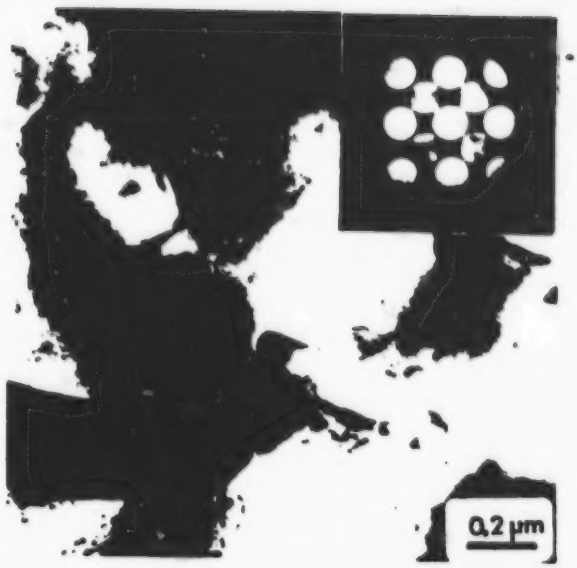

Figure 13: Micrograph of the interparticle areas after ageing showing precipitates approximately 0.2 µm in size formed in a matrix of almost pure zinc.